DC Current Measurement at Femtoampere Levels and Characterization of Thin, Coated Wires for *In Vivo* Applications

Jerry Martyniuk
Precision Interconnect, an AMP Company

ABSTRACT

Connections to biomedical sensor implants require wires or wire strands consisting of exceptionally small thinly coated conductors. This paper describes a method and instrumentation for measuring the DC leakage current through insulating layers of typically 2 to 25 µm in thickness on small-gauge wire (such as 25-µm gold). This involves current measurements in the low femtoampere (10^{-15} amperes) regime. To compare relative effectiveness of insulations, the bulk resistance of the layer calculated from these measurements is introduced. Steps for further optimization of the procedures and additional considerations regarding mechanical requirements and characterization are presented.

INTRODUCTION

Over the past 20 years there has been increasing research and commercial activity in the field of neural control, which concerns the exchange of information between conventional electronic circuits and living neural circuitry.[1-3] Such interfaces are vital for research into the normal functions of the nervous system and for the development of neural prostheses to replace diseased or damaged functional elements. Notable successes have ranged from the Nobel prize-winning studies of information processing in individual neurons of the visual cerebral cortex[4] to the restoration of useful hearing in patients with profound sensorineural deafness. One important challenge to developing such interfaces is the very small size of the functional units in the nervous system, i.e., individual neurons and their axons. Thus, the most crucial requirement imposed on a neural control interface is for one or more very small electrical probes that are stable in aqueous, saline solutions that can be placed close to individual neurons without excessive disruption of the surrounding tissue. Successful development of microelectrodes, with accurately exposed stimulation sites whose dielectric and conductive elements would not corrode or biodegrade *in vivo*, plays a major role in advancing toward the ultimate goal of providing sight, sound, and movement to the neurologically disabled. This technology also impacts efforts related to muscle stimulation, biosensing, and *in vivo* monitoring.

Along with probes and sensors, miniature wire assemblies must be developed. Since they are implanted in subdural material, it is vitally important that such assemblies not only be biocompatible and small but also very flexible, with their flex life comparable with the design life of the device. After completion of a feasibility study,[5] investigation of the electrical and mechanical properties of wire and coated wire for connection to neurological probes began. These studies are described here.

ELECTRICAL TESTING

Apparatus and Setup

The bulk resistivity of insulating materials suitable for the applications mentioned above is very high, typically 10^{14} to $10^{18}\ \Omega \cdot$ cm. Measurements are further complicated by the necessity of evaluating the performance of very thin coatings on small samples immersed in a saline solution. Thus, in order to compare the performance and stability of differ-

ent insulating materials, it was necessary to design and build equipment permitting (1) reliable resolution of current measurements well into the sub-pA regime; (2) minimization of external field effects; (3) minimization of temperature fluctuations; and (4) minimization of disturbance by external vibrations.

Figure 1 shows a schematic of the experimental setup; Figure 2 is a photograph of the temperature-controlled sample compartment. The additional requirement for the mathematical protocol to deal with varying thicknesses on different diameter wires is discussed separately below.

Measurements at the low current levels of interest are strongly influenced by noise. While refining the apparatus, it was found that most of the noise came from external vibration, which would manifest itself via capacitive coupling to the wires in the cage and produce electrical noise.[a] The system was stabilized by mounting the entire assembly on a mechanically isolated granite table and by using shielded leads, even in the innermost cage.

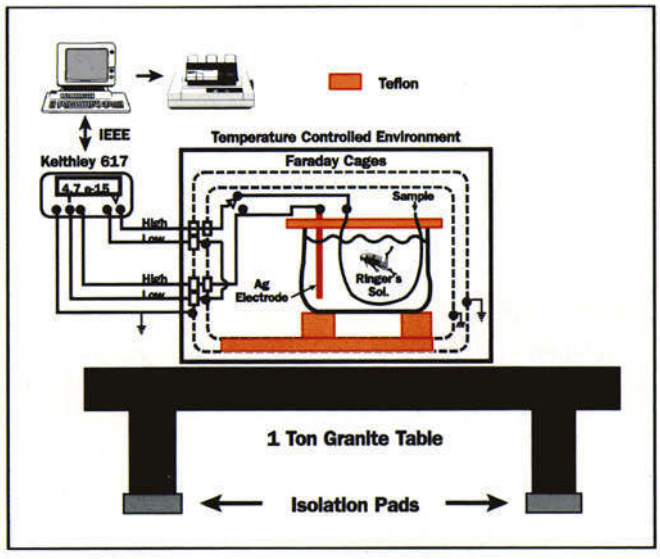

Figure 1. Schematic of the experimental arrangement, including circuitry.

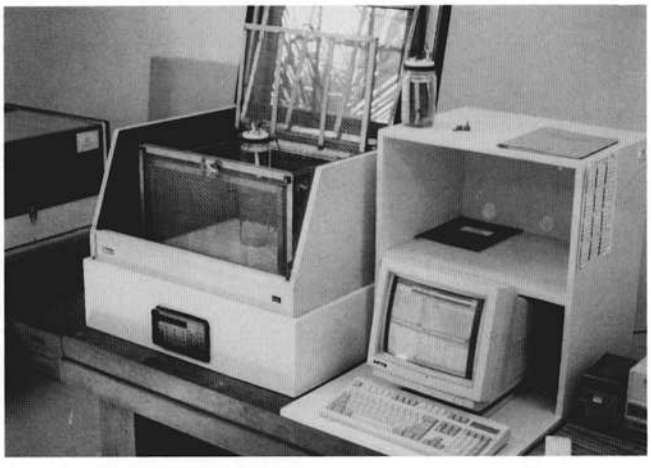

Figure 2. Photo of the environmentally controlled sample compartment.

Evaluation of Baseline Performance

To check the capability of the experimental arrangement, a Keithley 100-GΩ ± 2-percent resistor was placed in the cage and connected to the Keithley 617 electrometer (see Figure 1). The electrometer was adjusted to provide a 1-V bias. Before starting the measurements, the system was allowed several hours to reach equilibrium. Then, over a period of 36 hours, a total of 34,000 readings were made. This period was chosen to see if there was a night-day-night temperature fluctuation. An average current of 10.1788 pA (with a standard deviation of 1.83 fA) was measured. The distribution of the current readings is shown in Figure 3.

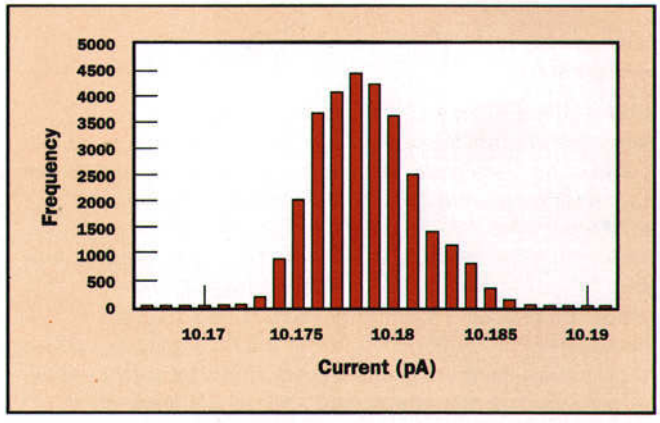

Figure 3. Keithley 617 electrometer current readings through a 100-GΩ resistor with a 1-V bias.

Assuming an error-free applied voltage of 1 V, the measured current of 10.1788 pA ± 1.83 fA would yield a resistance of 98.24 ± 0.02 GΩ. There are, however, thermoelectric offsets due to different temperatures of metallic junctions in the system. These must be eliminated, as well as any electrochemical offsets that would be incurred with the sample in a saline solution. A slope method, which is explained below and in Figure 4, serves this purpose.

Additional errors caused by noise and drift can be introduced into a system in four ways:

1. by the source
2. by the connections to the measuring instrument
3. in the measurement instrument

[a] Laboratory mythology has it that the setup appeared to be almost sensitive enough to determine mass, velocity, and color of trucks traveling on a nearby freeway.

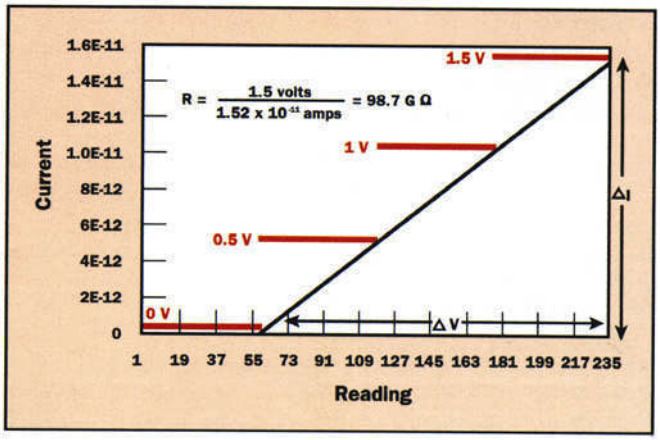

Figure 4. Current leakage through a 100-G Ω (± 2 percent) resistor. The wait period eliminated the exponential decay almost completely.

4. by extraneous disturbances, such as electrostatic and electromagnetic fields.[6]

The source noise, also known as Johnson noise I_J, can be calculated as the noise current developed in a resistance by

$$I_J = \sqrt{\frac{4 \cdot k \cdot T \cdot \Delta f}{R}} = 0.22\ [fA] \qquad (1)$$

where:

k = Boltzmann's constant = 1.38×10^{-23} J/K
T = temperature = 310K
Δf = noise bandwidth = 0.28 Hz for the Keithley 617 electrometer at 1 V, measuring currents of 10 pA.[8]

With these values, the Johnson noise current I_J in the 100-GΩ resistor is approximately 0.2 fA. Additional errors introduced by voltage and connection noise, extraneous disturbances, and instrument drift are not included in I_J. Since the setup was able to produce 36 hours of data with a standard deviation of 1.8 fA, which is about an order of magnitude above the Johnson noise floor, it was concluded that the poin of diminishing return had been reached regarding expense versus achievable accuracy.

Software Configuration

To handle the massive amounts of data, a Windows-based application using National Instruments' GPIB drivers was developed. The software is user-configured and permits selection of any measurement profile defined by the following set of variables: wait state, voltage, current window, and number of readings per hour and test duration.

Because of the long times required for reaching equilibrium after voltage changes, the program was written to give the user the choice of setting a wait time of up to one hour. During this period, the electrometer remains on the lowest impedance current measurement scale to aid in bleeding off injected charges. It was found that buried charges, caused for instance by voltage spikes or triboelectric effects, took hours to dissipate.

The data are taken off the electrometer in blocks of 100 readings at the rate of 30 seconds per block. This time increment is very small compared with the overall measurement time for a particular voltage, making it necessary to record only the average and the standard deviation of each block. The data is automatically compressed, loaded into Excel spreadsheet software, graphed, and logged into a workbook data file by month.

Measurement Method and Sanity Check

The resistance of the device under test (DUT) is determined by measuring the current through the sample at several different voltages and looking at the slope R = ΔE/ΔI for the DUT. This technique-eliminates-constant electromotive forces (emfs) generated by thermoelectric, electrochemical, and electromechanical effects, which can produce intrinsic voltage offsets depending on individual setup parameters. As a final sanity check for the overall setup and the software, the 100-GΩ resistor was connected as before but the voltage was changed in 0.5-V increments from 0 to 1.5 V. Figure 4 shows current vs. number, where each reading represents the average of a block of 100 individual readings. Note in Figure 4 that, as anticipated because of the presence of Seebeck (thermoelectric) emf in connections and electrochemical effects, the current is $I \neq 0$ for an external voltage E = 0 V.

As illustrated in Figure 4, the voltage change ΔE = 1.5 V produced a corresponding current change ΔI = 15.2 pA, indicating a resistance of

$$R = \frac{1.5\ [V]}{15.2\ [pA]} = 98.7\ [G\Omega] \qquad (2)$$

This value is slightly larger than the 98.24 GΩ found with a single measurement. The reason is that the single-point method failed to allow for current flow caused by temperature differences or electrochemical potentials in the system.

Once the resistance of the sample is known, one can calculate the *in situ* bulk resistivity ρ of the coating following a procedure discussed in Appendix A. A comparison of samples on the basis of their bulk resistivity has the advantage of being independent of coating thickness or wire diameter. Because the macroscopic bulk resistivities for the materials in question are fairly well known, the measured data compared to them can serve as indicators for the microscopic uniformity of the coating. For instance, measurements on a coating with pinholes, pores, or microcracks would yield a bulk resistivity much less than the expected value of 10^{14} to $10^{18}\ \Omega \cdot cm$.

Examples

The experimental arrangement of the sample and its immediate environment is shown schematically in Figure 5. A jar containing Ringer's solution (a conductive, aqueous saline solution) simulates to some extent the *in vivo* environment. A known length of the insulated conductor in question is immersed into the solution, leaving one bare end above the PTFE lid for termination at potential V_1. Via a platinum wire, the solution is set at V_0, the inner shield ground potential. The potential difference $E = V_1 - V_0$ drives the leakage current through the coating. After the jar is placed in the shielded test chamber shown in Figure 2 and the circuits are connected according to Figure 1, the electrometer monitors the current flowing through the wire insulation. The influence of external current paths or ground loops was minimized by using PTFE for all separations. It should be noted that at these current levels and because of the long duration of each measurement, even some glass jars (depending on their base composition, thermal history, and surface treatment) can sustain currents large enough to interfere with the measurement.

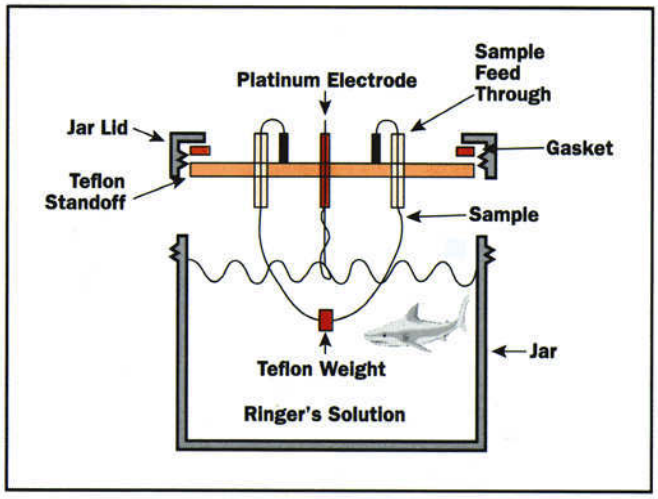

Figure 5. The test jar.

The sensitivity of the setup against temperature fluctuations was determined by monitoring the temperature of the liquid in the jar over an extended period of time. Although the temperature in the laboratory itself fluctuated between 24°C and 26°C, the thermal inertia of the jar combined with that of the mass of the saline solution was sufficient to hold the sample at a constant temperature of 25°C. Of course, different results have to be expected when the heater is used to keep cages and contents at body temperature, which is 37°C.

Like all other elements of the experimental setup, design and construction of the heating circuitry and the heater required special attention. Ideally one would desire no switching noise, no air currents, and no ungrounded sensing circuitry. Several approaches were tested. The heating device used now consists of a large aluminum plate as the environmental floor. It is equipped with Nichrome heating elements. The temperature of the plate is monitored continuously to maintain the enclosure at body temperature.

As discussed above, the magnitude of the actual voltage across the dielectric is $E = V_{applied} - V_{offset}$, where V_{offset} is a voltage originating from thermoelectric and electrochemical emfs within the system. Figure 6 shows that the current $I \neq 0$ for $V_{applied} = 0$, where $V_{applied}$ is the voltage applied by the electrometer.

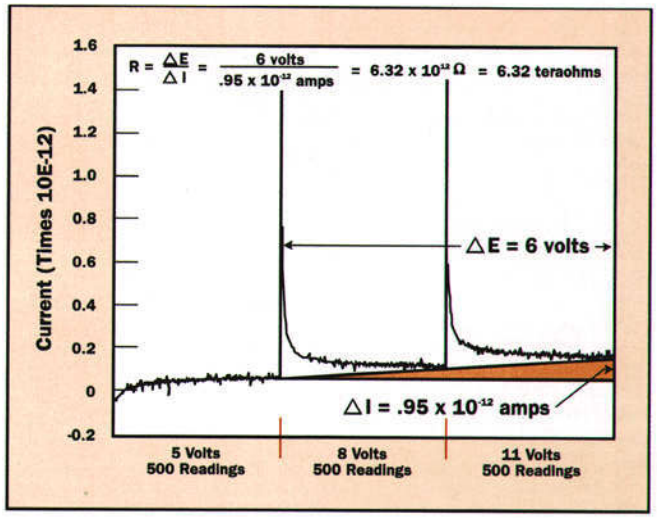

Figure 6. Leakage current, 32-μm (1.25-mil) thick platinum/iridium wire, 5-μm polyimide with 2-μm modified polyimide overcoat.

It is desirable to minimize the wait period between changes of $V_{applied}$. This is done by switching the electrometer to the mA scale where the meter impedance is lowest, so that equilibrium is reached most expediently. Figure 6 would illustrate an even more dramatic RC behavior if the segments of the graph depicting the wait state were included. Questions related to optimization of the wait period will be addressed more fully below.

Early in the development of the method most measurements showed a very small linear voltage vs. current relationship, even when the sample was disconnected. Thus, each measurement was repeated with the sample disconnected and the current measured under these conditions subtracted from the total current. As the experimental setup was improved—for instance, by using thoroughly cleaned PTFE—the background leakage current fell below the noise limit of the apparatus and could be ignored.

As mentioned already, data were recorded by taking blocks of 100 readings over approximately 30 seconds, the electrometer's limit. For these sets of data only the averages

and standard deviations were recorded. It was found that occasional spurious events would occur in which the current would jump to a much lower value for a few of the 100 readings. The software looked at each set of 100 readings, eliminated those that were more than three standard deviations away from the norm, and recalculated and recorded the new statistics.

Even though the actual dielectric leakage current is measured, the bulk resistivity p derived from it is more suitable as a figure of merit for comparing samples because it also accounts for material and thickness anomalies. For multistrand cables, effective areas for the current path have to be introduced. They depend on the geometry of the cable and have to be found separately for each configuration. For single strands, assuming that the dielectric is homogeneous, isotropic, and of uniform thickness, an expression for the effective bulk resistivity is derived in Appendix A with the result

$$\rho = \frac{2 \cdot \pi \cdot L \cdot R}{\ln(D1/D2)} \qquad (3)$$

Four different cable configurations were tested. Their cross-sections are shown in Figure 7. Although the geometry of samples (A) and (B) differs from that of samples (C) and (D), the magnitudes of the specific currents I/A_{eff} can be compared to characterize the effectiveness of the coatings. The effective area $A_{eff} = L \cdot \pi \cdot (D_2 - D_1)/2$. This formula applies to single-strand as well as multistrand wires because during the test only one strand located at the outside of the multistrand cable is at potential.

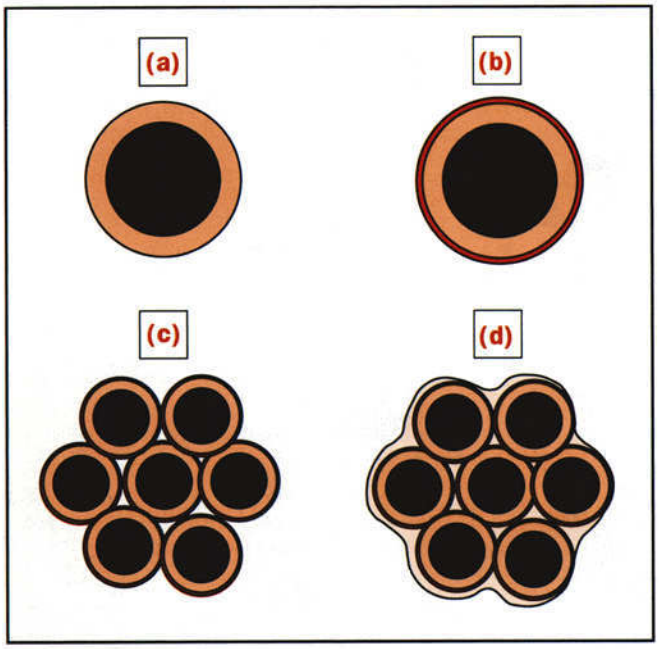

Figure 7. Wire configurations tested.

The results for sample (A) indicate that PTFE could serve as a most effective insulator. However, the surfaces of the samples studied were rough. This is not surprising, considering the known difficulties in producing consistently uniform coatings from PTFE, particularly at the sizes and thicknesses of interest here. The roughness of the surface would require introduction of an "effective thickness" smaller than that actually measured. This explains why the bulk resistivity derived from our measurements is at least an order of magnitude less than that reported in the literature.

The data in Table 1 show an increase in leakage current from single-strand to seven-strand modified polyimide-coated cables, although the opposite should be expected. Likely reasons for the increased leakage current are stresses and microcracks induced in the coatings during stranding. However, as the results on samples (D) show, an additional overcoat of modified polyimide can improve the level of leakage current to that of PTFE-coated, single-strand wires.

Table 1. Measured results.

Sample	$I/Area_{eff}$ fA/cm²@5V	ρ ohm-cm × 10^{15}	σ_ρ ohm-cm × 10^{15}
A 1)	pinholes		
2)	37	190	90
B 1)	232	30	12
2)	266	26	11
3)	269	26	14
C 1)	322	22	7
2)	282	25	12
3)	45	15	5
4)	381	18	5
D 1)	51	140	269
2)	121	58	45
3)	83	85	91
4)	62	114	162

ADDITIONAL CONSIDERATIONS

Electrical Measurements

Without changing the basic concepts and experimental arrangements, the procedure and to some extent the accuracy of the results could be improved. The following considerations address some of these points.

The sample itself forms an unshielded loop that couples capacitively to the cage walls. Because the cage walls do not shield magnetic fields effectively, the sample must also be expected to couple to stray magnetic fields. Despite the precautions already taken, these effects make the system susceptible to external vibrations and external magnetic fields.

A further complication is introduced by the need to carry out measurements at body temperature, which is about 12°C above laboratory temperature This involves switching a heater off and on, which in turn results in buildup and

breakdown of a magnetic field. To achieve rapid response to temperature adjustment calls, the heater has to be close to the sample, at least within the shielded cage. The end result is that the baseline resolution suffers a reduction of approximately an order of magnitude with a sample in place and the heat on.

At present, the resolution is adequate at these temperatures. If desired, the baseline can be lowered to a few femtoampere by increasing the magnetic isolation of the cage and modifying the switching circuitry for the heater.

Another major area of desirable and possible improvement is related to the time required for testing a sample. After switching to a new voltage, the system needs periods of 12 to 24 hours to reach equilibrium for low-leakage samples. Typically, three or more voltage levels are desirable for the determination of the bulk resistance: two of them to calculate the slope and at least one to establish slope redundancy. In this regard, the current vs. time relationship is studied in some detail, The initial parts of the I(t) curves are quite complex, but after about 20 minutes I(t) approaches an exponential decay function

$$I(t) = A + B \cdot \exp(-C \cdot t) \qquad (4)$$

where A, B and C are constants. Equation 4 describes a current flow with an initial current of (A + B) for t = 0 approaching exponentially a final value of A for $t \rightarrow \infty$ with a time constant (or relaxation time) of 1/C. Applied to a test case where the sample was heated and run for 32 hours producing the curve in Figure 8, the stable value A of the current was approximately 2.17 pA. The ripples in the curve are caused by the heater's turning on and off.

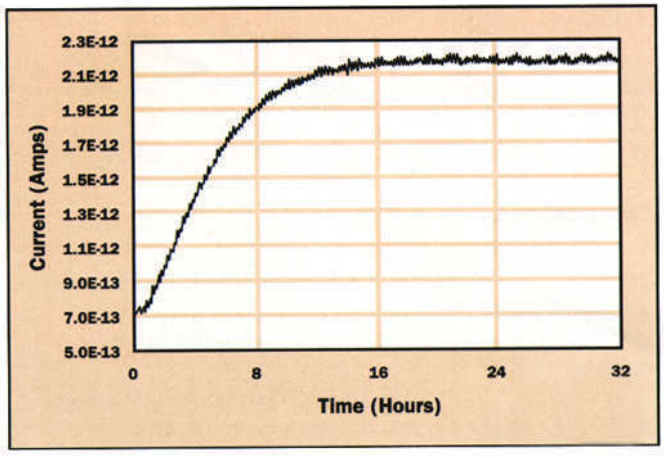

Figure 8. Modified polyimide, seven-strand leakage current.

Data accumulated during the first 8 hours were fitted to Equation 4 by Statgraphics software. Figure 9 gives a graphic representation of the results. Next, the entire set of data for the 32 hours was fitted to Equation 4 by Statgraphics and the coefficients for both fits tabulated in Table 2.

The constant A for the "best fit" of 8 hours of data was 2.29 pA; the "best fit" calculated from the set of 32 hours of data was 2.18 pA. The comparison of both sets leads to the conclusion that the test time could be reduced from 32 hours to 8 hours with a 5-percent error. Because of other error sources not covered in the discussions, this 5-percent error rate is a conservative estimate.

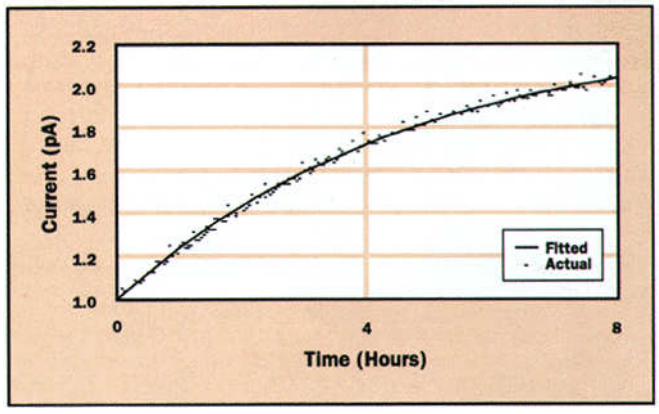

Figure 9. Eight hours of data fit to Equation 4 by Statgraphics.

Table 2. Best fit for $Y = A + Be^{ct}$ vs data.

	32 Hours		8 Hours	
	Value	σ	Value	σ
A	2.180	.001	2.287	.013
B	−1.176	.004	−1.243	.011
C	.011	.001	.009	.001

To reduce the duration of each test, the exponential fit to the data must be done in real time so that the program can decide when enough data has been taken and goon to the next voltage. With this in mind, a program described briefly in Appendix B was written to perform the fit. Preliminary studies indicate extremely acceptable performance.

Mechanical Measurements

In addition to these considerations, which address electrical metrology, mechanical performance of the leads must be evaluated. Because probes will often be in cerebral material while interfacing with fine wires to a location permanently attached to the skull, the flexibility and flex life of the wires and their coatings is an issue of paramount importance. To permit corresponding mechanical measurements, the sample jars were designed so that the wire sample can be flexed about an arbitrary radius while submersed in the solution at body temperature while a voltage is applied, without leaving the original jar. Figure 10 shows a schematic of the design. This allows samples to be retested electrically for leakage currents after flex testing. The number of flexures can be selected as desired, and

degradation of the insulative performance can be determined as a function of that number.

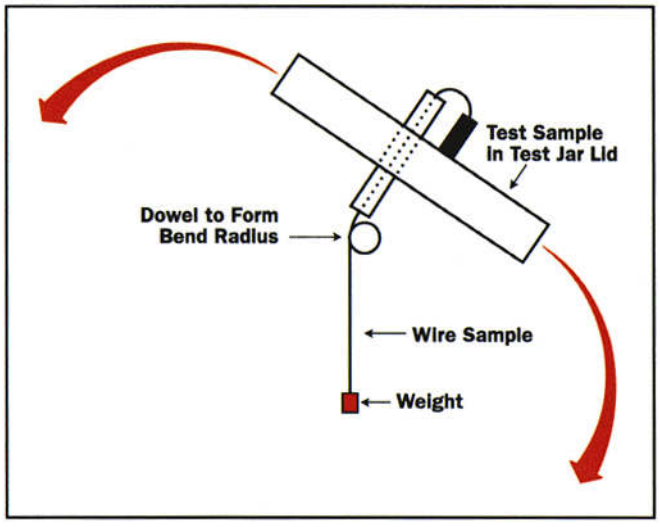

Figure 10. *In situ* flex tester.

Another aspect of the mechanical performance is the stiffness of the coated wires and cables. It is highly desirable that the probes be exposed to a minimum of force during cerebral movement to prevent post-installation trauma. A device shown schematically in Figure 11 was fabricated for clamping the test wire in a fixture, which was placed on a sensitive scale. By carefully moving an edge down against the wire at a predetermined position, the deflection of the wire is recorded. With the corresponding force determined by the scale, here serving as a load cell, and applying the well-known formula for a cantilever beam, the stiffness (or its reciprocal, the compliance) of the wire can be found. From it, an effective modulus of elasticity can be calculated.[9] The apparatus was sensitive enough to show the increased stiffness caused by thin insulating coatings applied to gold wires. This was shown to be valid even for low-modulus materials such as silicone rubber.

CONCLUSIONS

A complete environmental system for testing current leakage through coated wire samples was fabricated. The system is capable of resolving currents into the sub-pA regime. If used at temperatures above room temperature, the heating circuitry increases the standard deviation of the noise floor of a low leakage sample by about a factor of 5. DC offset in the system due to electrochemical and electromechanical effects is removed by computing resistance from the slope of voltage vs. current curves. The leakage current approaches its steady-state value exponentially. This behavior can be modeled quite accurately and utilized to shorten the time of testing by almost an order of magnitude with little sacrifice in accuracy.

Although it may seem that measurements of current at these levels are unrealistic or "overkill," it is of vital importance to see the actual amount of the leakage current in order to track items such as trending. For instance, in some of the coatings evaluated by others[10] the currents remained small at the pA level but showed a definite exponential rise, leading to catastrophic failure months later.

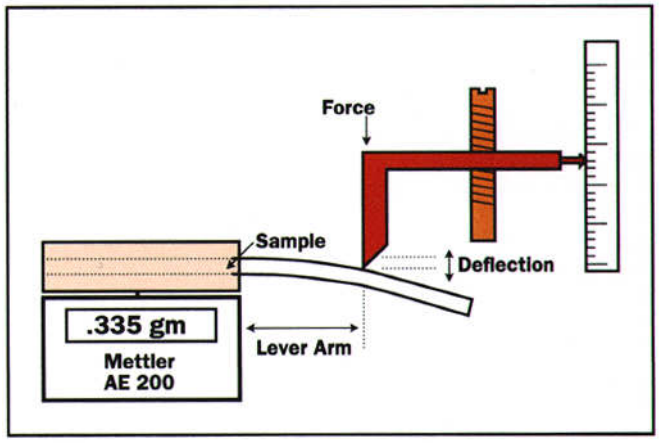

Figure 11. Apparatus for measuring elastic modulus of wire.

A method for comparing the flexibility of these miniature wires and coatings is outlined. The apparatus used for these measurements is sensitive enough to show the increased stiffness caused by thin insulating coatings applied to gold wires, even for low-modulus materials such as silicone rubber.

ACKNOWLEDGMENTS

I want to thank my colleagues at Precision Interconnect: Michael Demeter, for extensive software support and implementation; Scott Corbett, principal investigator on this grant, for advice and counsel; Dan Davis, for help with the graphics presentation; and Dan DeLessert, Dave Miller and other members of the laboratory for additional support. Thanks also to the National Institute of Health for funding of phases I and II of SBIR NIH N44-Ns-1-2319; and to Emil Deeg, AMP Incorporated Consultant, for providing stimulating conversations during the preparation of the manuscript.

APPENDIX A

Computing the Bulk Resistivity of Uniformly Coated Wires

Consider a conductor schematically shown in Figure 12 with circular cross-section of diameter D1 coated with an insulator of bulk resistivity p to a total thickness with outside diameter D2. The resistance of the insulating coat-

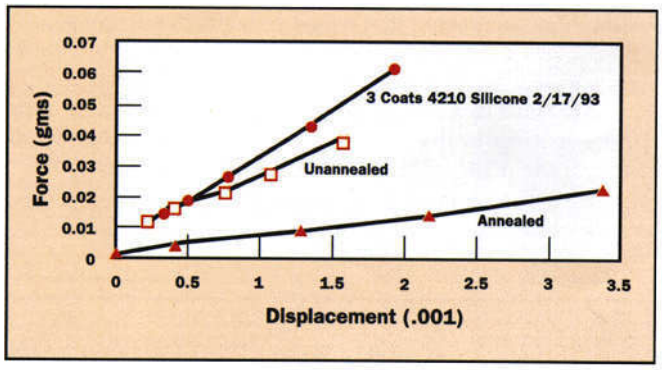

Figure 12. Force-displacement curves for 50 AWG gold wire.

ing is to be found for a length L with the coated wire submersed in a conductive solution.

Ohm's law in differential form, written for cylindrical coordinates and with j being the specific current, is

$$j = -\left(\frac{1}{\rho}\right) \cdot \nabla u = -\left(\frac{1}{\rho}\right) \cdot \left\{\frac{\partial u}{\partial r}; \frac{1}{r} \cdot \frac{\partial u}{\partial \varphi}; \frac{\partial u}{\partial z}\right\} \qquad (A1)$$

For an isotropic and homogeneous coating ρ is constant; for smooth surfaces, uniform thickness of the coating, and a straight wire, it is $\partial u/\partial \varphi = \partial u/\partial z = 0$. Thus, equation (Al) is reduced to

$$j = j_r = -\left(\frac{1}{\rho}\right) \cdot \frac{du}{dr} \qquad (A2)$$

Because of

$$j(r) = \frac{I}{A(r)} = \frac{I}{2 \cdot \pi \cdot r \cdot L} \qquad (A3)$$

it is

$$\frac{du}{I} = -\left(\frac{\rho}{2 \cdot \pi \cdot L}\right) \cdot \frac{dr}{r} \qquad (A4)$$

and after integration, replacing radii by diameters and because of E/I = R

$$R = \frac{E}{I} = \left(\frac{\rho}{2 \cdot \pi \cdot L}\right) \cdot \ln\left(\frac{D2}{D1}\right) \qquad (A5)$$

which yields equation (3) in the body of the paper:

$$\rho = \frac{2 \cdot \pi \cdot L \cdot R}{\ln(D2/D1)} \qquad (A6) = (3)$$

The effect of errors in individual quantities on the relative mean error of ρ is illustrated by

$$\left(\frac{\Delta\rho}{\rho}\right)^2 = \left(\frac{\Delta L}{L}\right)^2 + \left(\frac{\Delta E}{E}\right)^2 + \left(\frac{\Delta I}{I}\right)^2 + \left(\frac{1}{\ln(D1/D2)}\right)^2 \cdot \left[\left(\frac{\Delta D1}{D1}\right)^2 + \left(\frac{\Delta D2}{D2}\right)^2\right] \qquad (A7)$$

For very thin coatings, ln(D1/D2) assumes small values which can drastically increase the error contributions by D1 and D2. From Equation A6 the variance of ρ is found[11] as

$$\sigma_\rho^2 = \mathrm{Var}(\rho) = \rho^2 \cdot \left\{\frac{(\sigma_{\Delta I})^2}{(\Delta I)^2} + \left(\frac{D1}{D2}\right)^2 \cdot \left[\frac{\sigma_{(D1/D2)}}{\ln(D1/D2)}\right]^2\right\}$$

where

$\sigma_{(D1/D2)}$ = standard deviation of the diameter of the insulation assuming the wire diameter is constant, and

$\sigma_{\Delta I}$ = standard deviation of the change in current over the voltage range.

APPENDIX B

A Method of Real Time Curve Fitting

Write the data as

$$\mathrm{Ydata}_i = \mathrm{Current}(t_i) \qquad (B1)$$

For guess' on A, B and C compute the sum of squares error between the guess' and Y_{data}

$$SS = \Sigma\,\{\mathrm{Ydata}_i - [A + B \cdot \exp(-Ct_i)]\}^2 \qquad (B2)$$

Now treat the SS function as SS(A,B,C) and compute the direction d in ABC space of steepest descent which minimizes SS with respect to A, B, and C. It is[12]

$$d = \frac{-\nabla SS(A, B, C)}{\|\nabla SS(A, B, C)\|} = \hat{A}d_A + \hat{B}d_B + \hat{C}d_C \qquad (B3)$$

Now decide on the length of the step size λ to be taken in the direction **d** which minimizes SS. This is done by looking for a zero in the function

$$F_\lambda = \frac{\partial}{\partial\lambda}\{\Sigma\,[\mathrm{Ydata}_i - (A + \lambda \cdot d_A) + (B + \lambda \cdot d_B) \cdot \exp(-(C + \lambda \cdot d_C) \cdot t_i)]^2\} \qquad (B4)$$

which is done with a modified Newton's method. The values of A, B, and C are then replaced with $A + \lambda d_A$, $B + \lambda d_B$, and $C + \lambda d_C$, respectively, and the program returns to recompute a new SS error term according to Equation B2. It keeps repeating this process until the new SS term does

not improve by more than a preselected, arbitrary amount d from the previous iteration.

REFERENCES

1. G.E. Loeb, "Neural prosthetic interfaces with the nervous system," Trends in Neuroscience **12**(5),(1989).

2. E. Owens and D.K Kessler, *Coclear Implants in Young Deaf Children* (College Hill Press, Bristol, PA, 1989).

3. G.E. Loeb, "Progress Toward Visual Prostheses," Biomedical Engineering Unit, Queen's University, Kingston, Canada, 1990.

4. D.H. Hubel and T.N. Wiesel, "Receptive fields, binocular interaction and functional architecture in the cat's visual cortex," J. Physiol. 106-154, (1962).

5. S. Corbett *et al.,* "Miniature, Flexible Cable for *In vivo* Application," NIH contract N44-NS-1-2319, quarterly reports (1992/93).

6. C.D. Motchenbacher and F.C. Fitchen, *Low Noise Electronic Design* (Wiley, New York, 1973).

7. J.F. Keithley, J.R. Yeager and R.J. Erdman, "Low Level Measurements," Keithley Instruments, Inc. (1984).

8. J.R. Yeager, Keithley Instruments, Inc., private communication (1993).

9. E. Oberg *et al.*, *Machinery's Handbook*, 22nd ed. (Industrial Press, New York, 1984).

10. D. Eden, "Coatings for Protection of Integrated Circuits," 2nd Quarterly Report, NIH-NINDS-NOl-NS-2399 (U.S. Government Printing Office, Washington, DC 1991).

11. W.G. Hunter, J.S. Hunter, and G.E. Box, *Statistics for Experimenters* (Wiley, New York, 1978).

12. M.S. Bazaraa and C.M. Shetty, *Nonlinear Programming* (Wiley, New York, 1979).

Jerry Martyniuk is a Principal Engineer in the technology group at Precision Interconnect, an AMP subsidiary, in Portland, Oregon.

Mr. Martyniuk received a B.S. in physics from Portland State University in 1969, a M.S. in physics from University of Oregon in 1970, did research in theoretical solid state from 1970 to 1973 at the University of Oregon and received an M.S. in Electrical Engineering from Portland State University in 1990. He joined PI in 1990 where he has worked with lasers as applicable to wire stripping and micromaching as well as modeling the electrical behavior of coaxial type cables. Mr. Martyniuk is a member of The Optical Society of America (OSA), The Society of Photo-Optic Instrumentation (SPIE) and Pi Sigma Upsilon.